Opto-Electronics Review

journal homepage: https://journals.pan.pl/opelre

Infrared detectors: My scientific life

Antoni Rogalski

Institute of Applied Physics, Military University of Technology, ul. gen. Sylwestra Kaliskiego 2, 01-934 Warsaw, Poland

Article info

Article history:
Received 03 Jun. 2026
Accepted 26 Jul. 2026
Available on-line 11 Aug. 2026

Keywords:
infrared detectors;
HgCdTe;
PbSnTe;
QWIPs;
type-II superlattices;
low-dimensional solids

Abstract

My interest in infrared detectors began in 1970 while I was working on my master's thesis to complete my studies in technical physics at the Military University of Technology (MUT) in Warsaw (Poland). At that time, I was developing a photoconductive detector technology based on copper-doped gallium arsenide (GaAs:Cu). Even then, it was known that semiconductor compounds with a narrow energy gap were superior to doped semiconductors for infrared detector design because of their better physical properties. Throughout the 1970s, I worked on the technology, physical properties, and characterisation of lead-tin telluride photovoltaic detectors. However, the development of HgCdTe epitaxial technologies (LPE, MOCVD, and MBE) with optimal physical properties (particularly the absorption coefficient and carrier lifetimes), and a better-matched coefficient of thermal expansion to silicon signal readout processors in hybrid infrared arrays led to the discontinuation of further work on lead-tin telluride in the 1980s. For this reason, I turned my attention to solid-solution alternatives to HgCdTe (ZnHgTe, MnHgTe) and subsequently to semiconductor solid solutions of the A^{III}-B^{V} compound group, such as InAsSb and GaSb/InAs superlattices. My scientific achievements in this field of research were the basis for receiving the Foundation for Science Award (the most prestigious scientific award in Poland) in 1997. At the turn of the 20th and 21st centuries, I spearheaded the creation of a laboratory dedicated to the growth of HgCdTe epitaxial layers in partnership with Vigo System S.A. In 2003, we launched the MUT-Vigo HgCdTe MOCVD laboratory. A decade later, in 2015, I expanded our research to include second-type superlattices, specifically GaSb/InAs and InAs/InAsSb, by integrating MBE epitaxy into the joint laboratory. Over the past two decades, I have focused on a new generation of detectors based on low-dimensional solids, whose properties are governed by quantum-size effects. My contribution to this area of research focuses primarily on analysing the performance and role of the new generation of LDS photodetectors within the broad family of infrared detectors. This area of research, in turn, was honoured with the Prime Minister's Award in 2024.

1. Introduction

Numerous materials have been explored in the field of infrared (IR) technology. Examining the evolution of IR detector technology, a straightforward principle, based on Norton's paper [1], can be articulated: "*All physical phenomena in the range of about 0.1–1 eV can be proposed for IR detectors*". Among these phenomena are the following: thermoelectric effects (thermocouples), variations in electrical conductivity (bolometers), gas expansion (Golay cell), pyroelectric effects (pyroelectric detectors), photon drag, the Josephson effect (Josephson junctions, SQUIDs), internal emission (PtSi Schottky barriers), fundamental absorption (intrinsic photodetectors), impurity absorption (extrinsic photodetectors), low-dimensional materials [superlattice (SL), quantum well (QW), and quantum dot (QD) detectors, 2D materials], various types of phase transitions, and so on.

Figure 1 outlines the approximate timelines of key advancements for the materials discussed. The foundation

*Corresponding author at: antoni.rogalski@wat.edu.pl

https://doi.org/10.24425/opelre.2026.1616
1896-3757/ Association of Polish Electrical Engineers (SEP) and Polish Academy of Sciences (PAS). Published by PAS
© 2026 The Author(s). This is an open access article under the CC BY license (https://creativecommons.org/licenses/by/4.0/).

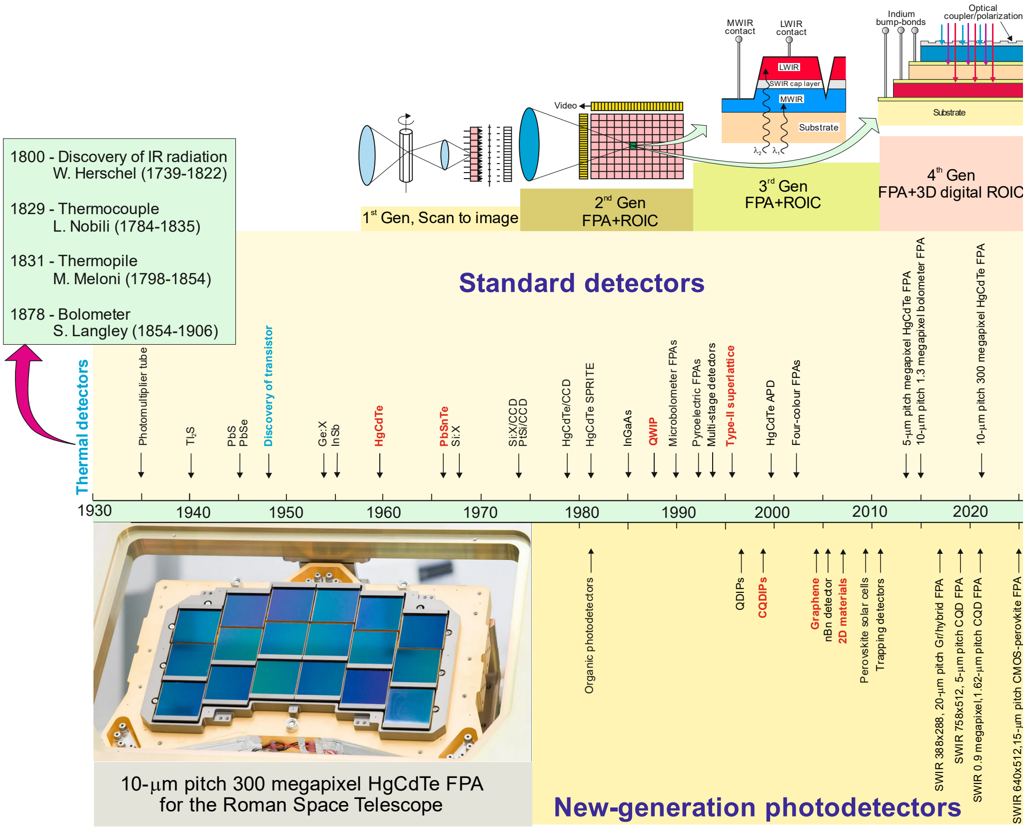

Fig. 1. The evolution of IR detectors and systems can be categorised into four generations, each serving key military and civilian purposes. The first generation comprises scanning systems, while the second generation includes electronically scanned staring systems. The third generation features staring systems with a high pixel count and dual-colour capabilities. Finally, the fourth generation encompasses advanced staring systems with many pixels, multi-colour functions, and additional on-chip features, such as improved radiation-to-pixel coupling, avalanche multiplication within pixels, and polarisation and phase sensitivity. The IR materials I have studied over the past five decades are marked in red. The image at the bottom left shows the largest HgCdTe detector array intended for installation in the Roman Space Telescope.

of contemporary IR detector technology dates to World War II. Innovations in IR technology, advancements in semiconductor materials, and photolithography techniques originally designed for integrated circuits, along with motivations stemming from Cold War military readiness, have collectively led to remarkable progress in IR capabilities over the last seven decades. Recent technological advances have led to detector designs that boost device sensitivity, improve frequency response, minimise noise levels, and expand the gain bandwidth.

The identification of graphene (Gr) and other two-dimensional (2D) materials has sparked significant interest in a new wave of optoelectronic devices during the last two decades (marked as *New generation photodetectors* in Fig. 1), offering a foundation for diverse photonic applications, particularly in high-speed photodetectors. Artificial intelligence (AI) is increasingly paired with imaging technology in various autonomous systems for detecting signals. Notably, sensors that operate in the longer-wave IR and terahertz ranges can effectively capture images even in challenging outdoor conditions, such as inclement weather or nigh time. When integrated with AI, these systems can analyse incoming images and generate appropriate responses. Therefore, AI plays a crucial role in enhancing image interpretation.

My work in the field of IR technology dates to 1970, so it has been over 50 years since I first began working on IR photon detectors. Five years earlier, in 1965, G. E. Moore, co-founder of Intel, published a paper that laid the groundwork for the famous Moore's Law [2], which remained in effect until around 2020. It notes that the number of transistors on a microchip tends to double about every two years, leading to a reduction in computer costs by half during the same period. This exponential advancement has driven significant increases in computing power, reductions in size, and greater affordability over the decades, serving as a guiding goal for the semiconductor sector.

Moore's Law has significantly advanced thermal imaging systems. The progress of these imaging systems is facilitated by silicon integrated circuit (IC) technology ability to read, process array signals, and render the resulting images. As shown in Fig. 2, array sizes have evolved over the last 60 years. Focal plane arrays (FPAs) are developing at a pace similar to that of dynamic random-access memories (DRAMs), although they were about a decade behind. While array sizes will continue to expand, the growth rate will fall short of that predicted by Moore's Law. This pattern has been apparent for the last ten years, as indicated by the diamond-shaped data points in Fig. 2. Although increasing array sizes remains technically possible, the market forces that once drove the push for larger arrays have weakened, especially after surpassing the megapixel sensor threshold.

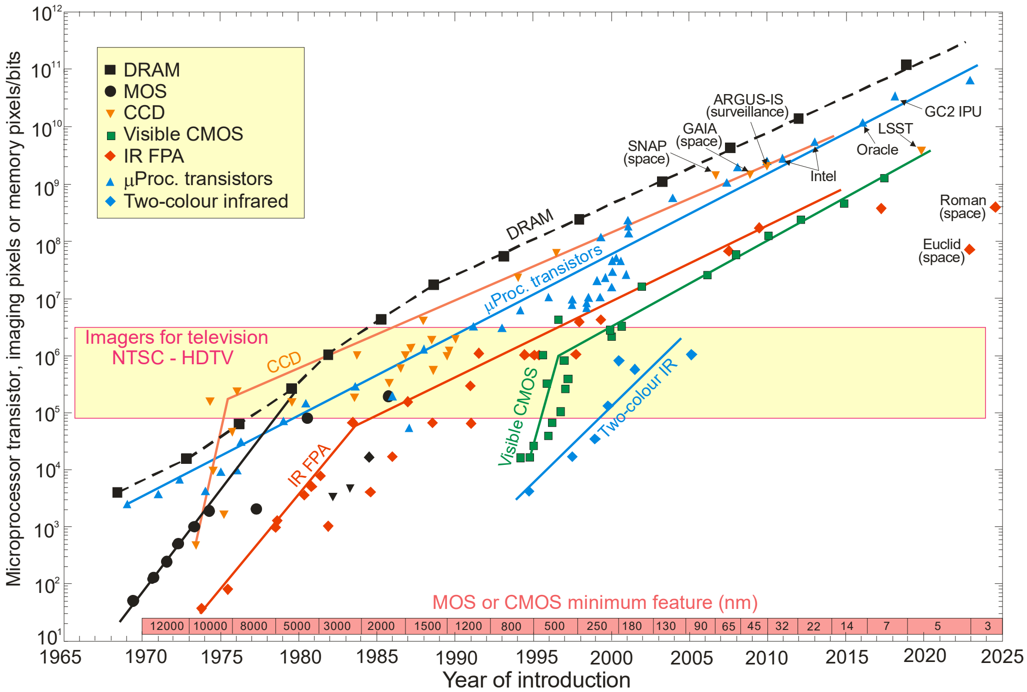

Fig. 2. The evolution of image sensors is highlighted alongside that of silicon microprocessors and dynamic random-access memory (DRAM), both characterised by the number of transistors and memory capacity. A timeline of the design rules for MOS/CMOS technology is presented at the bottom. Notably, CMOS sensors operating in the visible spectrum have rapidly advanced and now outperform CCD devices. Additionally, large IR sensor arrays with more than 100 megapixels are available for astronomical research. Many sensor types now have matrix formats that surpass those used in high-definition television.

2. Master's thesis

The aim of this thesis was to develop a detector sensitive to CO_2 laser radiation, discovered in 1964 by Patel [3] – the first molecular laser emitting a wavelength of 10.6 µm. It was a photoconductive detector made of copper-doped gallium arsenide (GaAs:Cu). However, its spectral sensitivity was low (Fig. 3) [4]. The detection limit at room temperature was 3.7×10^6 cmHz$^{1/2}$/W at 7.3 µm, which is two orders of magnitude lower than that of thermal detectors. A slight detector sensitivity at 10.6 µm was observed at the edge of the decline in photosensitivity. Even then, it was known that narrow gap intrinsic semiconductors are well-suited as active materials for IR detectors operating in the 8–14 µm atmospheric window. One of these materials was the ternary alloy mercury-cadmium telluride (HgCdTe) system discovered in 1959 [5]. Discovery of HgCdTe provides an unprecedented degree of freedom in IR detector design. In 1966, another ternary alloy system based on lead-tin telluride (PbSnTe) was discovered [6].

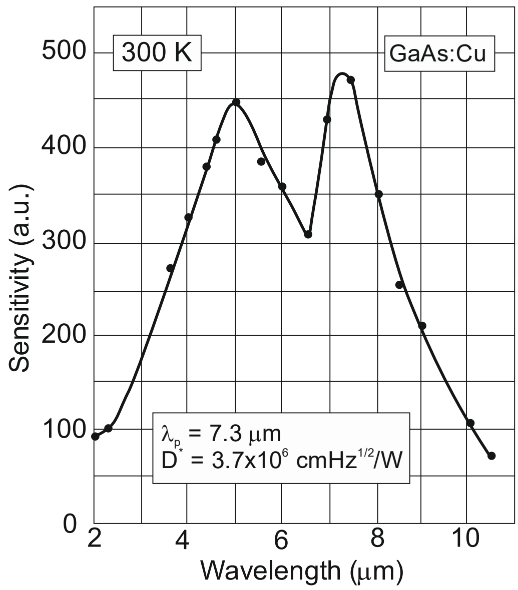

Fig. 3. Spectral dependence of sensitivity for copper-doped gallium arsenide (GaAs:Cu) photoconductive detector (after [5]).

3. Lead salts

During the 1970s, PbSnTe was a strong competitor to HgCdTe in terms of IR detector performance. For this reason, many research centres worldwide began studying lead salt compounds for their suitability as active materials for IR photodiodes. I joined this new field of research and conducted it for the next decade – until around 1980. My papers published at that time were not recognised in the global literature due to legal regulations imposed by the Ministry of National Defence (resulting from the East-West confrontation during the "Cold War"). These strict regulations were "relaxed" at the turn of the 1970s and 1980s. However, to publish papers in a Western journal, I had to obtain the Deputy Minister of National Defence's permission.

I chose a modified hot-wall evaporation (HWE) technique for growing lead salt films belonging to $A^{IV}B^{VI}$ material systems [7, 8]. The advantage of the HWE technique is the ability to prepare high-quality films with a composition close to stoichiometry [9]. These epitaxial films were prepared mainly on lattice-matched BaF_2 and KCl substrates at low growth temperatures in a relatively short time. They do not require additional annealing to improve their quality. Moreover, by controlling the vapour pressure of one of the components of the deposited material, it is possible to obtain films with a p-n junction.

Figure 4(a) shows the HWE system [10]. The space between the source and substrate was surrounded by a hot quartz channel. A quartz baffle placed inside the channel improves the conditions for thermodynamic equilibrium of the evaporated molecules. The system was provided with two independent sources of PbSnTe (or PbTe) and Te. The deviation from stoichiometric composition of the film was controlled by the temperature of the tellurium source. The heater substrate was placed directly above the channel open end.

The high quality of the $Pb_{1-x}Sn_xTe$ layers was confirmed by X-ray analysis, and their high carrier mobility (above 1000 cm^2/Vs and 20 000 cm^2/Vs at 300 K and 77 K, respectively). Using high-quality PbSnTe layers deposited on various substrates, I conducted pioneering research on their optical properties in the mid-1970s. I determined the relationship between the energy gap and composition within the range of $0 \le x \le 0.30$. Based on the positions of the interference maxima in the transmission spectrum of the epitaxial layers in the IR range from 4 to 20 µm, I determined the refractive indices of $Pb_{1-x}Sn_xTe$ with various compositions, x. I also estimated the high-frequency dielectric constant for these compositions. The results of the above studies are shown in Fig. 5. Using refractive index dispersion in the long-wavelength range:

$$n^2 = \varepsilon_\infty\left(1 - \frac{\omega_p^2}{(2\pi c)^2}\lambda^2\right), \quad (1)$$

where ω_p is the plasmon frequency, c is the speed of light, and λ is the wavelength, the linear portion of the long-wavelength region of the curve, extrapolated to zero wavelength, gives $\varepsilon_\infty = n^2 = 31.9$, 34.5 and 37.0 for $x = 0$, 0.19, and 0.29, respectively.

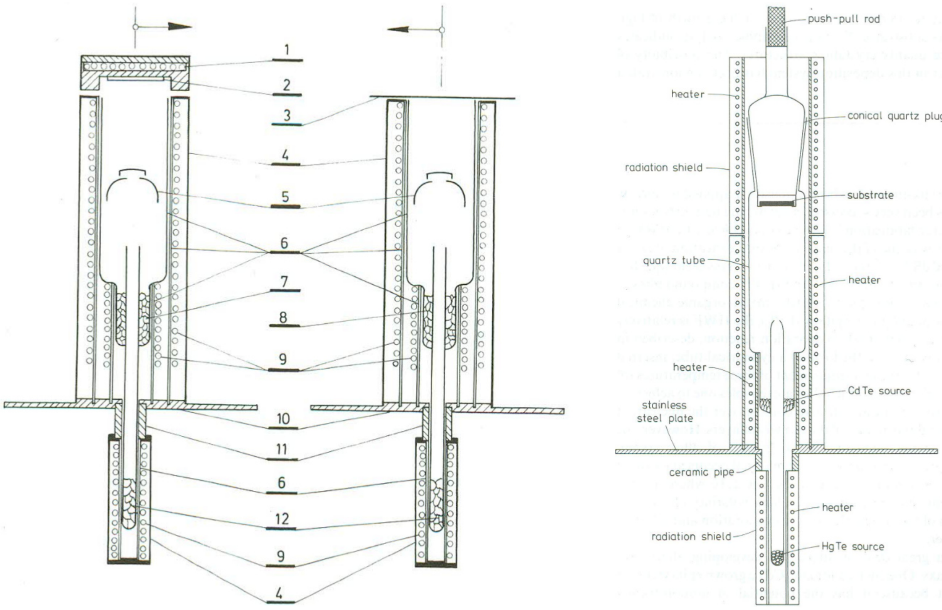

(a) (b)

Fig. 4. Modified hot-wall evaporation (HWE) technique: (a) schematic diagram of the experimental arrangement for the preparation of n-PbTe/p-$Pb_{1-x}Sn_xTe$ heterojunctions: 1) tantalum substrate heater; 2) substrate; 3) sliding shutter; 4) stainless steel heat radiation reflector; 5) baffle; 6) quartz tube; 7) $Pb_{1-x}Sn_xTe$ source charge; 8) PbTe source charge; 9) tantalum heater; 10) stainless steel plate; 11) ceramic tube; 12) tellurium reservoir (after [10]); (b) HWE system for depositing CdTe and HgCdTe layers (after [11]).

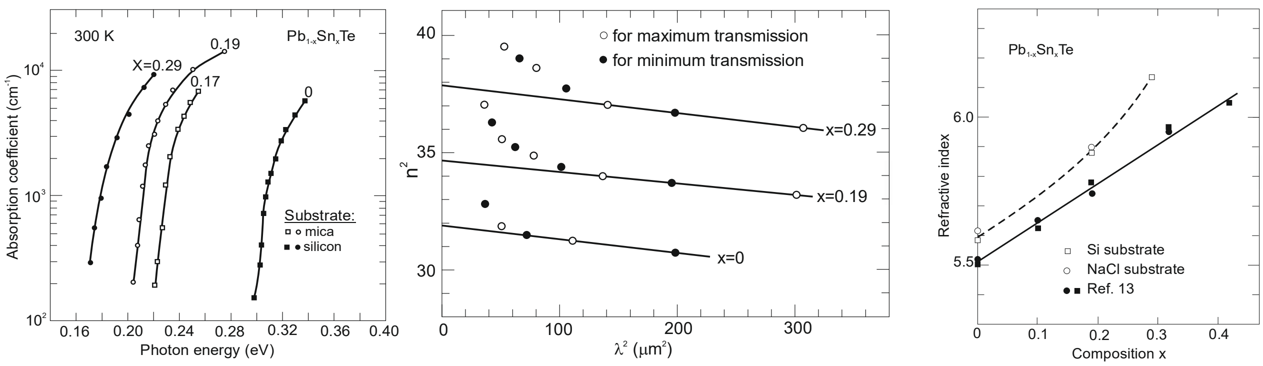

(a) (b) (c)

Fig. 5. Optical properties of $Pb_{1-x}Sn_xTe$ layers at room temperature: (a) absorption coefficient, dependence of n^2 on λ^2, and (c) refractive index (after [12] and [13]).

Using the HWE technique, n-PbTe/p-PbSnTe heterostructure photodiodes were produced that operate in the 3–5 µm and 8–14 µm atmospheric windows [10, 14, 15]. Their mesa structure is shown in Fig. 6(a). Initially, as a substrate, p-type PbSnTe monocrystals fabricated by the Brigman-Stockberger technique with a hole concentration of about 10^{19} cm^{-3} were used. On such substrates, n-type PbTe HWE layers deposited at substrate temperature of 280–300 °C with a thickness of about 5 µm were fabricated [14]. Figure 6(b) shows an example of the relative photosensitivity of a photodiode at temperatures 80, 197, and 300 K. The mesa-type photodiodes operated at about 80 K were characterised by a R_0A product of about 180 Ωcm^2, and the cut-off wavelength was shifted to 6 µm. Due to relatively high values of self-diffusion coefficients in PbTe and PbSnTe, the shift of the p-n junction from the PbTe/PbSnTe interface inside the PbTe layer was possible.

Similar results for n-PbTe/p-$Pb_{1-x}Sn_xTe$ heterojunctions with a long wavelength spectral cut-off ($\lambda_c \approx 6$ µm at 77 K) were obtained using the double-channel hot-wall technique shown in Fig. 4(a) [10]. In this case, first proposed by me, a 7–10-µm thick p-type $Pb_{1-x}Sn_xTe$ layer was deposited on a specially prepared substrate (BaF_2 or a PbSnTe monocrystal). Immediately after this process, *in-situ* (without breaking the vacuum), the substrate with the heater was shifted over the outlet of the second channel to evaporate an n-type PbTe layer. It should be noted that the double-channel hot-wall technique was later used to fabricate PbTe/PbSnTe superlattices [16, 17].

Table 1 collects properties of n-PbTe/p-PbSnTe mesa heterojunctions. Their performance was comparable to that presented in the 1970s for HgCdTe photodiodes.

Attempts to fabricate n-PbTe/p-PbSnTe heterojunction photodiodes operating in the 8–12 µm spectral range using the modified hot-wall technique have encountered certain difficulties. Diffusion processes at the PbTe/PbSnTe interface appear to be the main obstacle, and their influence depends on the carrier concentrations in PbTe and PbSnTe. Especially under the conditions used for PbSnTe layer deposition, the HWE system does not fully ensure precise control of the carrier concentration and layer composition. Although full reproducibility of the R_0A product was not achieved, and the spectral sensitivity characteristics shifted toward shorter wavelengths, photodiodes with cut-off wavelength close to 10 µm and an R_0A value equal to 1.1 Wcm^2 were demonstrated. They were characterised by a quantum efficiency of 30–40%, and high detection sensitivity (see Table 1).

4. Lead salts *vs.* HgCdTe

Lead salt ternary alloys offer several theoretical benefits when compared to HgCdTe:

- they have stronger chemical bonding,
- they show increased resilience to defects, as demonstrated in Fig. 7, which illustrates the correlation between the R_0A product and dislocation density for photodiodes with a 10 µm cut-off wavelength at 77 K,
- their cut-off wavelength is considerably less influenced by changes in composition,
- they require less stringent passivation, potentially allowing for the creation of larger and more uniform FPAs that can operate at higher temperatures.

These properties may have considerable effects, particularly in the long-wavelength IR spectral range. Nevertheless, there are still some challenges to address, including the material softness, its elevated dielectric constant (which slows down response speed), and a more pronounced thermal mismatch with silicon.

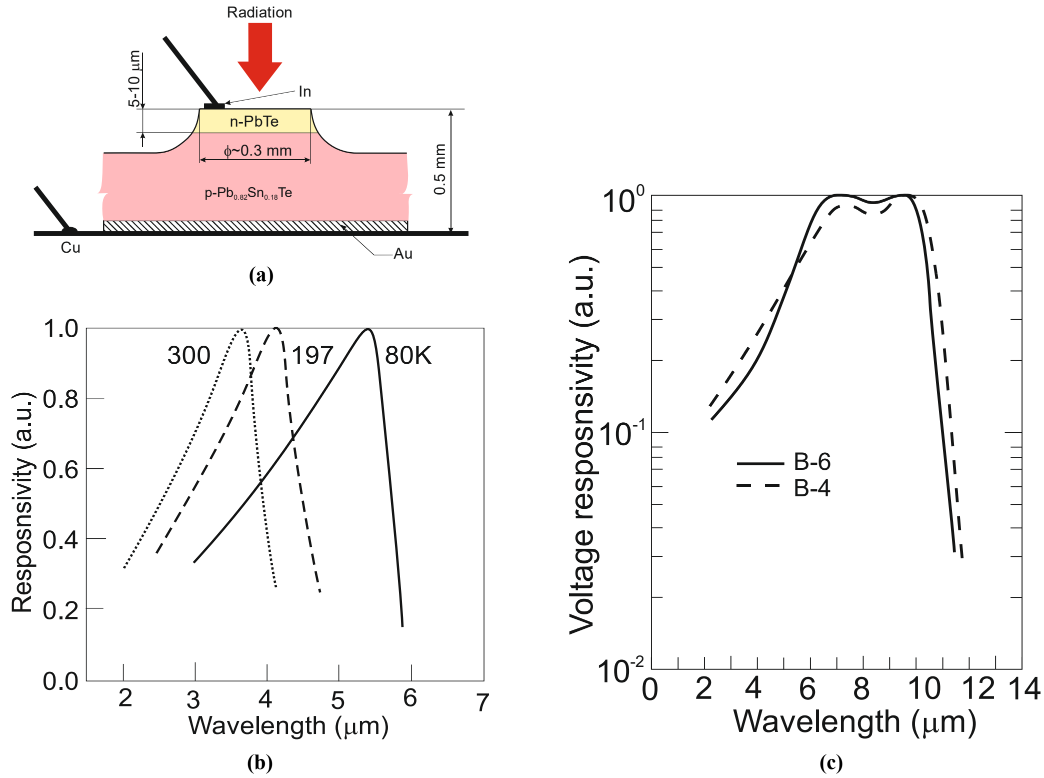

Fig. 6. n-PbTe/p-PbSnTe mesa photodiodes: the device structure (a); relative spectral characteristics in middle IR wavelength (b) [14] and long-wavelength (c) [15] IR windows.

Table 1.
Properties of n-PbTe/p-PbSnTe heterojunctions (after [10] and [15]).

Diode number	Temperature (K)	λ_{max} (μm)	R_0 (Ω)	R_0A (Ωcm^2)	η (%)	D^* (cmHz$^{1/2}$/W)
n-PbTe/p$^+$-PbSnTe heterojunctions						
C-1	77	5.3	140 000	175	28	2.4×10^{11}
	197	4.1	46	0.06	9	
	300	3.6	8	0.010	3	
C-2	77	5.3	110 000	140	35	2.7×10^{11}
	197	4.1	40	0.05	12	
	300	3.6	9	0.011	4	
C-3	77	5.3	80 000	100	40	2.6×10^{11}
	197	4.1	35	0.05	11	
	300	3.6	9	0.011	5	
C-4	77	5.3	70 000	88	17	2.3×10^{11}
	197	4.1	60	0.08	9	
	300	3.6	12	0.015	4	
n-PbTe/p-PbSnTe heterojunctions						
B-1	77	9.8	880	1.1	33	3.7×10^{10}
B-2	77	9.8	720	0.9	32	3.3×10^{10}
B-3	77	9.8	1120	0.8	30	3.0×10^{10}
B-4	77	9.7	650	0.8	34	3.3×10^{10}
B-5	77	9.8	650	0.6	35	3.0×10^{10}
B-6	77	9.5	320	0.4	38	2.7×10^{10}

The detectivity limit, D^*, is determined by Johnson noise.

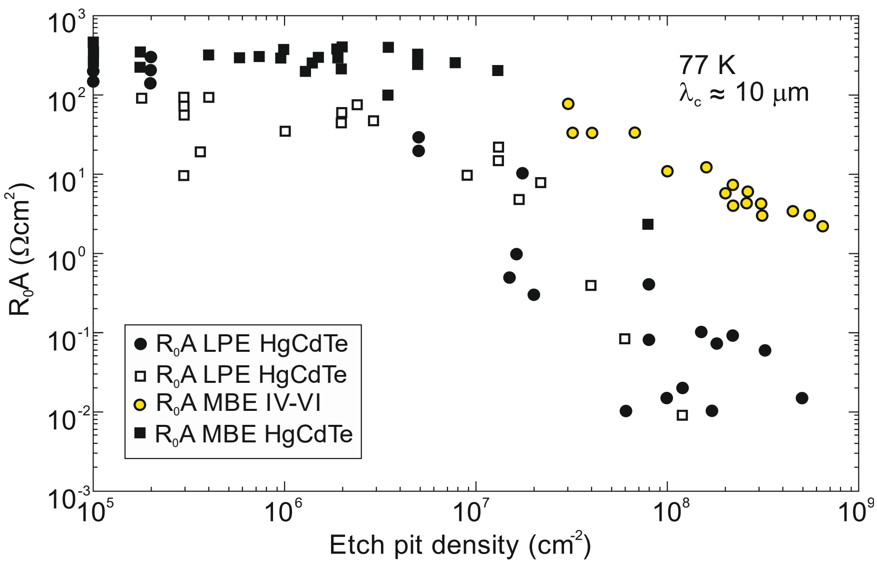

Fig. 7. Dependence of the R_0A product on dislocation density for HgCdTe and IV-VI photodiodes with cut-off wavelength ≈ 10 μm at 77 K.

Ternary lead salts, including PbSnTe and PbSnSe, are typically easier to manufacture and exhibit improved stability. However, progress in IV-VI alloy photodiodes stalled in the 1980s due to two main challenges associated with chalcogenides: their high dielectric constants (several hundreds) and elevated thermal coefficients of expansion (TCEs). The high dielectric constant increases the capacitance of the space-charge region, thereby reducing the photodiode response speed. Moreover, a high TCE creates difficulties to produce large FPAs. Figure 8 demonstrates how the thermal expansion coefficients of PbTe, InSb, HgTe, and Si change with temperature [18]. At room temperature, HgTe and CdTe display TCEs of about 5×10^{-6} K^{-1}, whereas PbSnTe has a TCE close to 20×10^{-6} K^{-1}. This leads to a significant disparity with silicon, which has a TCE of approximately 3×10^{-6} K^{-1}. Furthermore, both germanium (Ge) and gallium arsenide (GaAs) exhibit TCE values comparable to those of HgCdTe, suggesting that these materials can be used as substrates for growing epitaxial layers of HgCdTe.

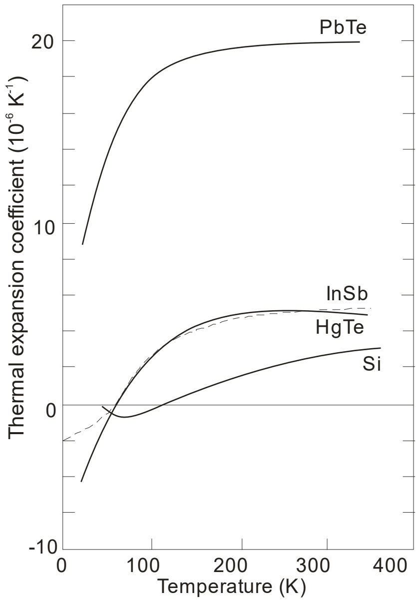

Fig. 8. Linear TEC of PbTe, InSb, HgTe and Si *vs*. temperature (after [18]).

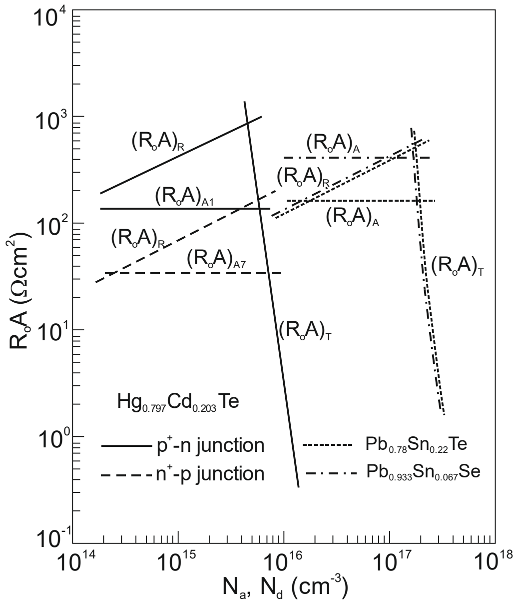

Fig. 9. The dependence of the R_0A product components on the dopant concentrations for the one-sided abrupt junctions produced in $Hg_{0.797}Cd_{0.203}Te$, $Pb_{0.78}Sn_{0.22}Te$, and $Pb_{0.933}Sn_{0.067}Se$ (after [19]).

The doping concentrations in the base regions of HgCdTe and PbSnTe photodiodes are notably different, as shown by Rogalski and Larkowski in 1985 [19]; see Fig. 9. To achieve high R_0A products, HgCdTe photodiodes need doping concentrations around 10^{16} cm^{-3}, while lead salt photodiodes require concentrations of 10^{17} cm^{-3} or lower. The maximum doping levels at which tunnelling onset occurs are considerably higher in IV-VI compounds than in HgCdTe. This is due to their higher permittivities, as the tunnelling contribution to the R_0A product involves factors expressed as $\exp[\mathrm{const}(m^*\varepsilon_s/N)^{1/2}E_g]$. Compared with HgCdTe detectors, lead salt detectors face performance limitations primarily due to the presence of space-charge region (SCR) centres. The precise origin of these centres is not entirely clear, but they likely stem from intrinsic or residual defects in the material. Lead salt detectors exhibit a dominant depletion current, unlike HgCdTe detectors with similar band gaps. As a result, lead salt detectors must operate at lower temperatures to achieve background limited IR photodetection (BLIP) performance. Moreover, Figure 9 shows that in p$^+$-on-n junctions with a thick n-type active region, the lower mobility of holes leads to a reduced minority-carrier diffusion length. This results in a higher diffusion-limited R_0A product than for n$^+$-on-p junctions. These theoretical insights were later supported by experimental findings from p-on-n HgCdTe junctions [20].

5. Commercialisation of HgCdTe detectors in Poland

The commercialisation of IR detectors in Poland started in the early 1980s, initially at the Institute of Plasma Physics and Laser Microfusion, and later at Vigo System S.A., a medium-sized company founded in Warsaw in 1987 [21]. Research and development primarily targeted the uncooled market segment. Despite extensive efforts over the years, no cost-effective technology was available to grow the HgCdTe base material. Initially, methods such as bulk growth and isothermal vapour-phase epitaxy (ISOVPE) in sealed ampoules were used, but these approaches proved inconvenient and expensive. A significant advancement was made with the introduction of an open-tube growth method. Professor J. Piotrowski, in collaboration with Djuric's team at the University of Belgrade [22], developed an innovative atmospheric-pressure production system – see Fig. 10. This reusable system allows for the growth of extensive areas with multiple layers in a single process run. It minimises mercury loss by employing a quartz assembly with a sealed container fitted with a conical quartz plug, resulting in only a few milligrams of mercury lost per run. The band gap profiles can be finely tuned by adjusting growth conditions and applying post-growth annealing. Depending on the growth parameters, layers can be created with thicknesses ranging from less than 1 micron to over 1 millimeter, and with a wide variety of surface compositions ($0 < x < 1$). To achieve excellent lateral uniformity ($x < 0.005$), temperature variations in the growth zone must remain below 0.3 °C.

The primary disadvantage of HgCdTe ISOVPE is the inherent difficulty in achieving uniform composition and thickness across large-area wafers. Because the growth

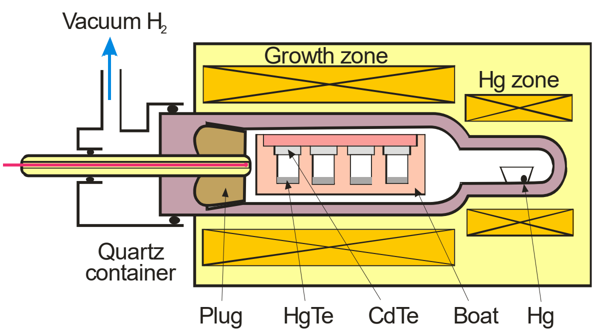

Fig. 10. Isothermal vapour phase growth reactor. Low-cost polycrystalline HgTe sources and large-grain CdTe (or CdZnTe) substrates were used (after [21]).

relies on solid-state interdiffusion between source materials and the substrate, controlling composition gradients remains a significant challenge. Also, my attempts to use modified HWE with a conical quartz plug [as shown in Fig. 5(b)] also failed to yield positive results [11].

At the turn of the 20th and 21st centuries, I initiated the establishment of a laboratory for the growth of HgCdTe epitaxial layers in collaboration with Vigo System S.A. In 2003, the joint MUT-Vigo HgCdTe MOCVD laboratory was established (MUT – Military University of Technology) (Fig. 11). A decade later, I began expanding research into second-type superlattices (GaSb/InAs and InAs/InAsSb) by installing MBE epitaxy in a joint laboratory in 2015. In hindsight, this was a very good decision. A model of cooperation emerged in which the commercial company focused on implementation, while the academic team focused on fundamental research.

I believe we serve as a good example of successful collaboration between science and innovative business – a model that continues to work to this day. We formed joint teams and projects, funded by both the National Science Centre (NCN), the National Centre for Research and Development (NCBR), and other agencies. The result was the emergence of Polish IR detectors based on III-V compound superlattices on the global market. For example, Figure 12 demonstrates the vertical cascade photodetector based on an InAs/InAsSb T2SL absorber, a bulk barrier layer, and a highly doped InAs/InAsSb T2SL n^+-p^+ tunnel contact junction [23]. The detector structure was grown by MBE on a buffered 1.1 mm GaAs (001) substrate. The Si donor and Be acceptor dopants were used.

As shown in Fig. 12(a), the detector consists of several layers, including a 250 nm GaAs smoothing layer, a 1-µm thick GaSb buffer layer that was deposited using the interfacial misfit (IMF) technique, and a 0.2 µm graded InAs/InAsSb N-layer that functions as both the electron contact and hole barrier. Additionally, there is a 0.62-µm thick InAs/InAsSb absorber made up of a 9.99 nm period of T2SLs consisting of InAs (7.58 nm) and InAsSb (2.41 nm), with $x_{Sb} = 0.38$. The structure further includes a 0.2 µm barrier and a 0.12 µm InAs/InAsSb p^+-layer, which serves as the hole contact. The neighbouring stages are interconnected by a tunnel junction comprising approximately 130 nm-thick p^+ and 45 nm-thick n^+ T2SL layers, which share the same design as the active layer but are heavily doped, with doping concentrations of $N_a \sim 2 \times 10^{19}$ cm^{-3} and $N_d \sim 10^{19}$ cm^{-3}. The device also features a heavily doped T2SL p^+-contact layer at the end.

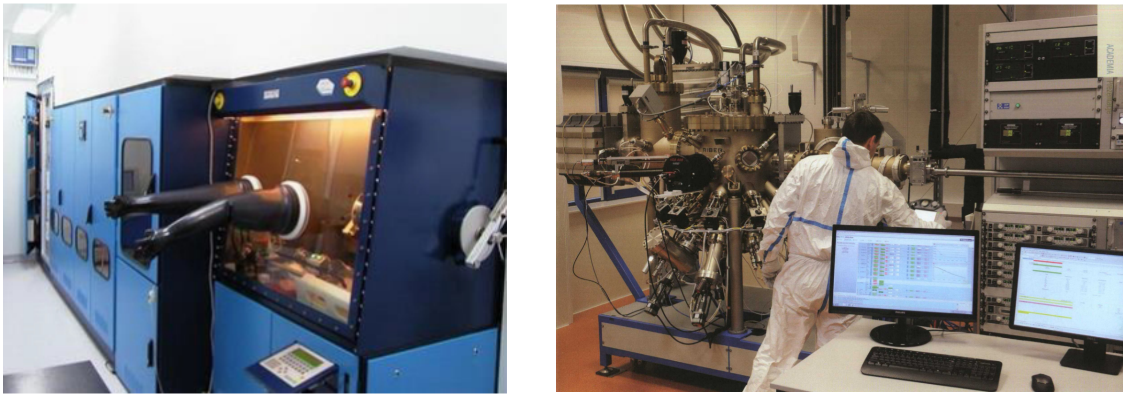

(a) (b)

Fig. 11. MOCVD HgCdTe Aixtron AIX-200 (a) and MBE Type-II SLs Riber Compact 21 DZ, (b) epitaxy systems in the MUT-Vigo laboratory.

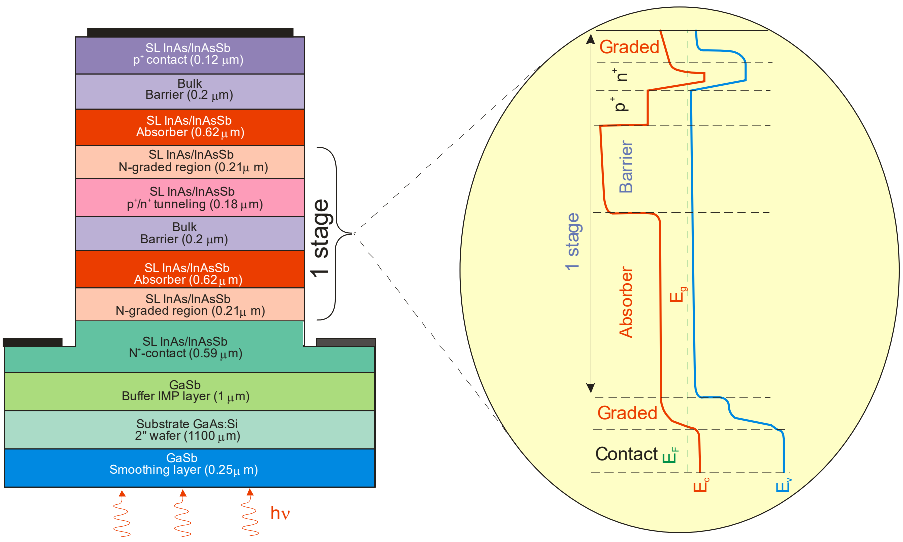

Fig. 12. The multi-stage LWIR InAs/InAsSb T2SL cascade photodetector: (a) detector architecture with p^+-n^+ connecting regions, (b) schematic of the energy band diagram with p^+-n^+ tunnelling region under unbiased conditions.

Figure 13 provides a comparative summary of the performance of multistage T2SL photodetectors operating at 300 K across a broad range of IR wavelengths. The detectivity of the hyperhemispherically immersed 3-stage heterostructure InAs/InAsSb interband cascade IR photodetector (ICIP) at a wavelength of $\lambda = 10.6$ µm achieves a level of 3×10^8 Jones at room temperature. This indicates a tenfold enhancement in detectivity compared to devices without an immersion lens, as well as a 30-fold increase in D^* in comparison to the 1-stage device with a net active layer thickness of 2.2 µm, which is comparable to that of the 3-stage cascade detector [24].

ICIP T2SL $A^{III}B^V$ photodetectors perform similarly to HgCdTe photodiodes. However, the development of ICIPs faces considerable challenges due to their complex manufacturing process, which involves multiple interfaces and stressed thin layers, as well as prohibitive costs.

6. New ternary alloy systems for IR detectors

In the late 1980s, I became interested in investigating alternatives to HgCdTe, particularly focusing on ternary alloys such as $Hg_{1-x}Zn_xTe$ (HgZnTe) and $Hg_{1-x}Mn_xTe$ (HgMnTe), as well as III-V compounds, especially those that utilize InAs [25–27]. My interest in HgZnTe and HgMnTe was driven by the challenges faced when attempting to produce high-quality HgCdTe crystals. A primary concern is the weak bond between mercury and tellurium, which leads to instability in the material bulk, surface, and interfaces. Achieving uniformity and a high yield is particularly difficult in the very long-wave infrared (VLWIR) spectral range. The difficulties in growing HgCdTe are attributed to the separation of the solidus and liquidus phases, leading to significant segregation between CdTe and HgTe, as depicted in Fig. 14. Moreover, the high vapour pressure of mercury further complicates growth. Among the small gap semiconductors derived from HgTe, HgZnTe, and HgMnTe stand out. In the case of the third ternary alloy based on HgSe, a significant hurdle in advancing $Hg_{1-x}Cd_xSe$ technology is achieving type conversion.

In 1985, Sher *et al.* [28] reported, through theoretical analysis, that the weak bond in HgTe becomes unstable when alloyed with CdTe, whereas it is stabilised when combined with ZnTe. Despite this, HgZnTe and HgMnTe have not been extensively researched for their use in IR detectors. This is attributed to several reasons. First, investigations into these alloy systems began after the advent of HgCdTe detectors. Furthermore, introducing HgZnTe poses more significant technological challenges than HgCdTe. Regarding HgMnTe, since manganese (Mn) is not considered a group II element, HgMnTe does not fit the criteria of a true II-VI alloy. This has led to scepticism among those unfamiliar with its crystallographic, electrical, and optical properties. As a result, those advocating for the advancement of both HgZnTe and HgMnTe for IR detector production have faced considerable challenges in securing support from industry players and funding agencies. During the 1980s, photodiodes based on both ternary alloy systems did not outperform those based on HgCdTe [27].

A III-V detector technology offers advantages such as enhanced bond strengths and material stability compared to HgCdTe, along with well-controlled dopants and high-quality substrates. The $InAs_{1-x}Sb_x$ ternary alloys, which hold the record for the lowest energy gap among III-V semiconductors, have a long development history. Woolley and his team first explored their properties in the 1950s [29]. InAsSb was introduced as a potential alternative to HgCdTe for IR applications in the mid-1970s [30]. However, advancements in this alloy system have been limited by challenges in crystal synthesis. The significant gap between the solidus and liquidus phases [see Fig. 14(b)],

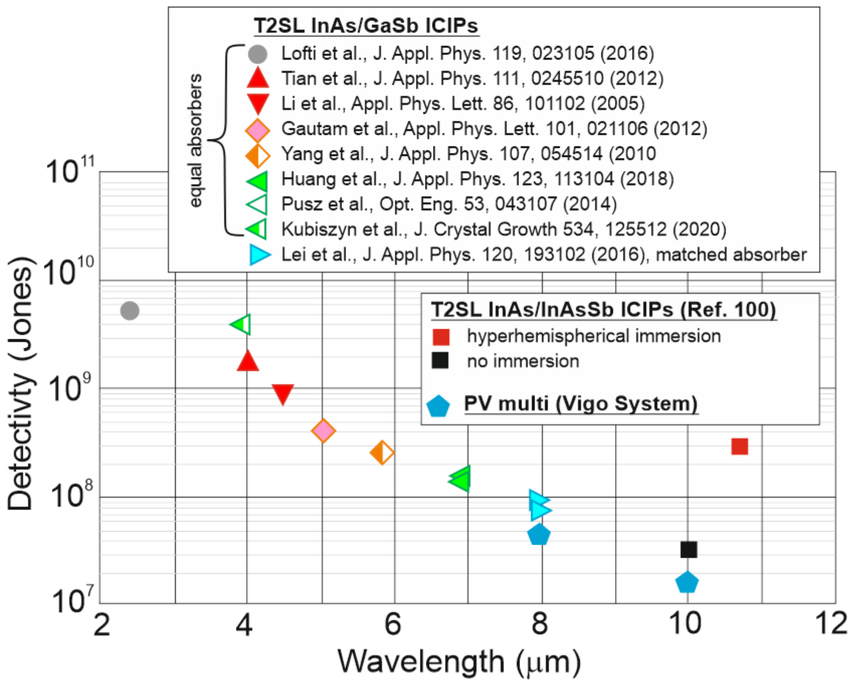

Fig. 13. Detectivity comparison *vs*. wavelength for T2SLs InAs/InAsSb-based ICIPs (without immersion and with GaAs hyperhemispherical immersion lens), T2SLs InAs/GaSb equal and matched-absorbers ICIPs, and HgCdTe-based multi-junction PVM detectors designed for 300 K.

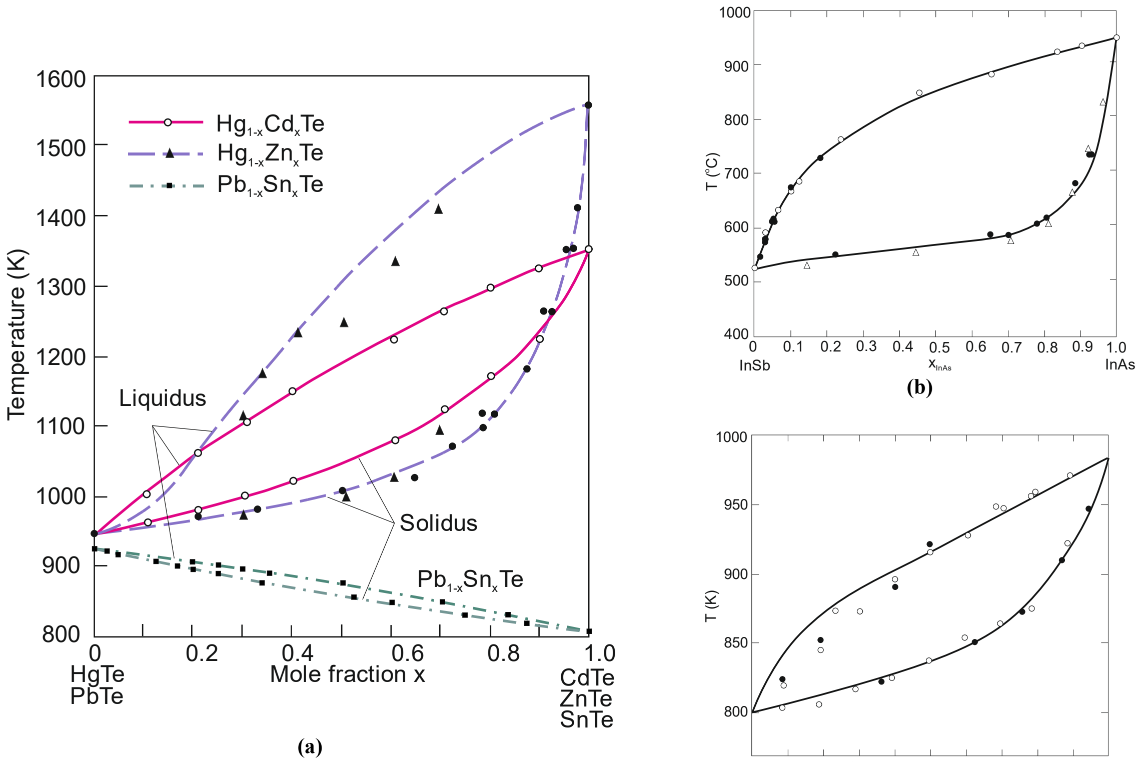

Fig. 14. Pseudo binary phase diagrams: (a) HgTe-CdTe, HgTe-ZnTe, PbTe-SnTe; (b) InSb-InAs; (c) InSb-GaSb.

along with a 6.9% lattice mismatch between InAs and InSb, imposes stringent requirements on effective crystal growth techniques. In 1989, I reviewed the initial progress in developing methods for growing InAsSb crystals, characterising their physical properties, and fabricating detectors [31]. At the time, I did not foresee that InAsSb would eventually play a critical role in the field. Ironically, my earlier paper, which seemed insignificant at the time, has turned into an important reference for foundational research over the years. Recently, there has been noteworthy progress in crystal growth methods and detector fabrication for $InAs_{1-x}Sb_x$, especially following the discovery of a new IR detector design that uses barrier detectors and type-II superlattices [32].

As I mentioned earlier, it was not until the mid-1980s that I was able to freely publish my papers in international scientific journals. A paper of over 200 pages published in 1988 in *Progress in Quantum Electronics* marked the beginning of my recognition as an expert in the field of IR detectors [33]. Other important monographs published in the subsequent period are shown in Fig. 15.

In 1997, I was awarded the Prize of the Foundation for Polish Science (FPS – the most prestigious scientific award in Poland) in the field of technical sciences for achievements in the study of ternary alloy systems for IR detectors – see Fig. 16.

7. New dimensional solids for IR detectors

Since Esaki and Tsu introduced the concept of semiconductor superlattices (SLs) and molecular beam epitaxy (MBE) became accessible in 1970 [35], interest in these materials has grown continuously. This heightened interest stems from technological challenges, groundbreaking physical ideas, and promising applications. Consequently, a new category of materials and heterojunctions with distinctive electronic and optical attributes has emerged. In this section, I will focus on devices that use IR excitation to generate carriers in low-dimensional solids (LDSs), including quantum wells, quantum dots, superlattices, and 2D materials. I will also discuss my contributions to these fields. One of the main advantages of

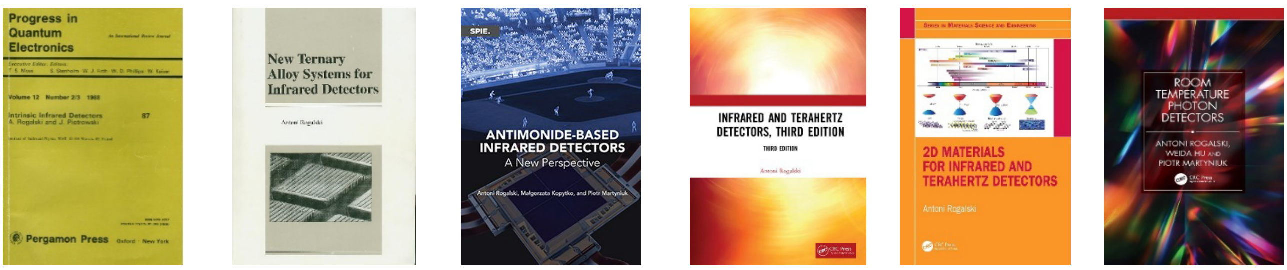

Fig. 15. Major monographs published between 1988 and 2025.

Fig. 16. Prof. A. Rogalski, winner of the 1997 FPS Annual Award, during the award ceremony at the Royal Castle in Warsaw (after [34]).

these IR detectors is that they can be made from chemically stable wide-band gap materials. Additionally, LDS materials exhibit physical properties that differ significantly from those of traditional crystalline materials, with their remarkable electrical and optical characteristics arising from quantum confinement effects.

7.1. Quantum well IR photodetectors (QWIPs)

Among the various types of quantum well IR photodetectors (QWIPs), the GaAs/AlGaAs multiple-quantum-well detector technology is the most well developed [36]. Compared with HgCdTe detectors, GaAs/AlGaAs quantum well devices offer several benefits. These include the use of conventional manufacturing techniques based on established GaAs growth and processing methods, as well as the ability to achieve uniform and precisely controlled MBE growth on GaAs wafers larger than 6 inches. Consequently, these factors contribute to higher production yields, reduced manufacturing costs, enhanced thermal stability, and greater radiation resistance.

Rogalski [37] employed straightforward analytical formulas for the detector parameters, following Andersson's paper [38]. In Fig. 17, the relationship between detectivity and long-wavelength cut-off for GaAs/AlGaAs QWIPs is illustrated at various temperatures. The experimental results demonstrate a strong correlation across a broad spectrum of cut-off wavelengths ($8 \leq \lambda_c \leq 19$ µm) and temperatures ($35 \leq T \leq 77$ K). This strong correlation holds true despite differences in doping levels, crystal growth methods (MBE and MOCVD), spectral widths, excited states (including continuum, bound, and quasicontinuum), and the inclusion of a different material system (InGaAs) in one instance.

Figure 18 [39] provides a clearer understanding of how dark currents vary with temperature by comparing current density with the inverse temperature for both GaAs/AlGaAs QWIPs and HgCdTe photodiodes, each with a cut-off

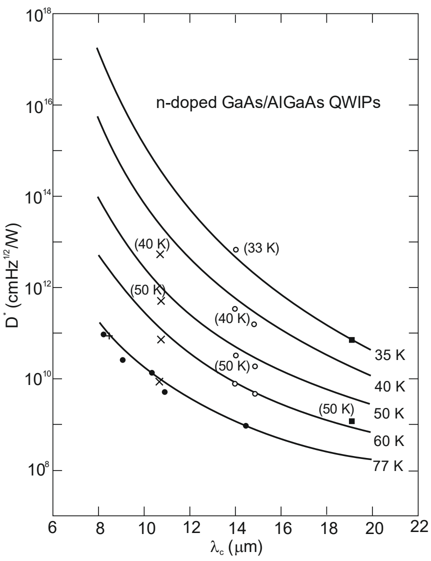

Fig. 17. Detectivity *vs*. cut-off wavelength for n-doped GaAs/AlGaAs QWIPs at temperatures ≤ 77 K. The solid lines are theoretically calculated. The experimental data are taken from different papers (after [37]).

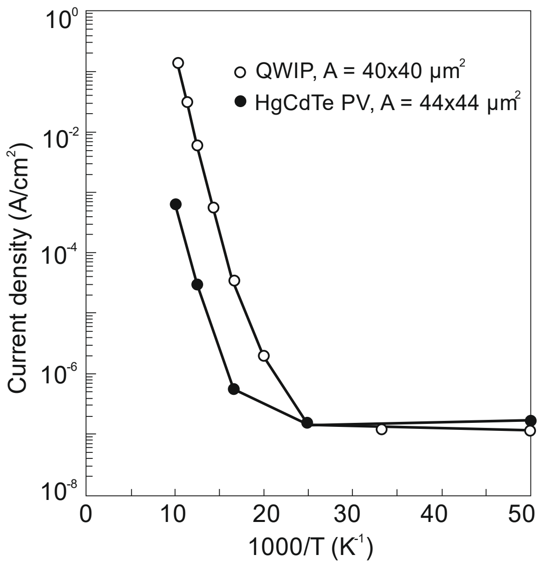

Fig. 18. Current density *vs*. temperature for a HgCdTe photodiode and a GaAs/AlGaAs QWIP with $\lambda_c = 10$ µm (after [39]).

wavelength (λ_c) of 10 μm. Below 40 K, both detector types show comparable current densities, as they are influenced by tunnelling effects that do not change with temperature. In contrast, when the temperature reaches 40 K or higher, the QWIP shifts into a thermionic emission mode, which is strongly temperature-dependent and increases rapidly. At 77 K, the dark current density for the QWIP is roughly two orders of magnitude greater than that of the HgCdTe photodiode.

LWIR QWIPs do not match the performance of HgCdTe photodiodes when used individually, especially at temperatures above 70 K. This is primarily due to difficulties related to intersubband transitions. Furthermore, QWIPs often show low quantum efficiencies, typically under 10%. In Fig. 19, the spectral quantum efficiency (η) of a HgCdTe photodiode is contrasted with that of a QWIP. Although QWIPs offer advantages such as stable pixel performance and the ability to create large arrays, they also have limitations, particularly in applications that require short integration times and must operate at lower temperatures than HgCdTe at similar wavelengths.

7.2. *Type-II superlattice detectors*

Over the last twenty years, antimonide-based FPA technology has achieved performance that rivals that of HgCdTe. A promising new approach involves utilizing type-II superlattices (T2SLs), which consist of both InAs/GaSb and InAs/InAsSb superlattices, along with barrier structures such as the nBn detector. These innovations aim to minimise generation-recombination leakage mechanisms and incorporate multistage/cascade IR devices [32].
In 2006, Martyniuk and I anticipated that T2SLs would be excellent candidates for third-generation IR detectors [40]. Figure 20 illustrates the R_0A values for InAs/GaInSb SLs and HgCdTe photodiodes in the long-wavelength range. The upper line indicates the theoretical performance limit based on diffusion, which relates to the Auger 7 limitation found in p-type HgCdTe materials. Figure 20 shows that the results for SLS photodiodes closely match those of established HgCdTe devices. At present, numerous manufacturers worldwide provide superlattice IR arrays that have performance capabilities on par with those of HgCdTe.

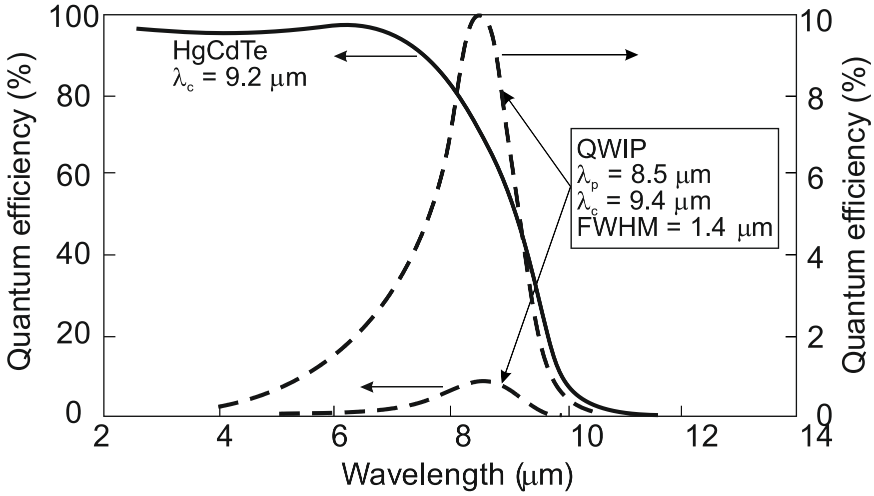

Fig. 19. Quantum efficiency *vs*. wavelength for a HgCdTe photodiode and GaAs/AlGaAs QWIP detector with similar cut-offs.

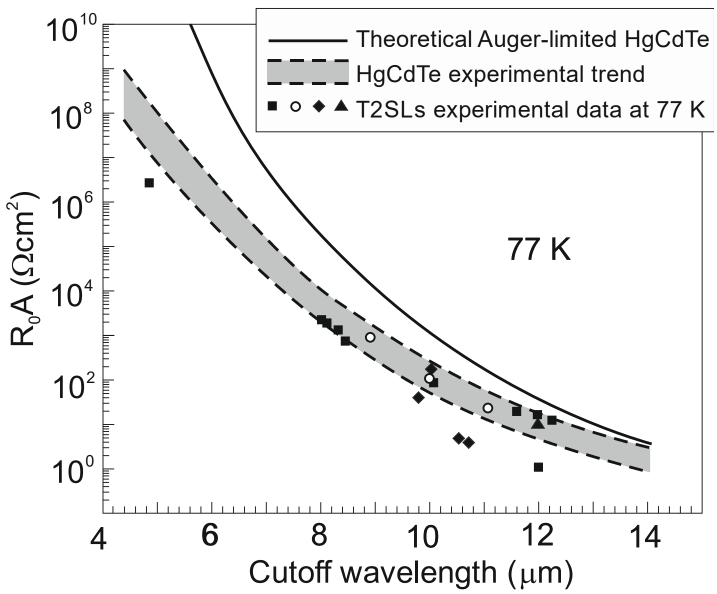

Fig. 20. Dependence of the R_0A product of InAs/GaInSb SLS photodiodes on a cut-off wavelength compared to theoretical and experimental trendlines for comparable HgCdTe photodiodes at 78 K. The experimental data are taken from various papers (after [40]).

7.3. a/G reference benchmark

This section summarises my perspective on the performance of new-generation IR detectors, primarily based on colloidal quantum dots, 2D materials, nanowires, perovskites, and organic photodetectors. The results presented here have been published in numerous papers over the past decade. The most important of these are [41–51]. In 2024, I was awarded the Prime Minister's Prize for scientific achievements in the field of innovative research on quantum detection structures for electromagnetic radiation across a broad spectrum, from the ultraviolet to the terahertz range [52].

Recent developments in IR detectors have led to innovative architectures that boost sensitivity, optimise frequency response, minimise noise, and expand gain bandwidth. Current research is primarily concentrated on three main advancements: smaller pixel sizes, high-operating-temperature (HOT) detectors, especially in the IR spectrum, and the use of AI. Increasing the operating temperature reduces strain on the detector cooling system, thereby enhancing its reliability. Moreover, AI is being integrated with imaging technology in various autonomous systems to improve signal detection. AI-based adaptive sensor systems may significantly enhance real-time image processing, refine signal interpretation, and facilitate bio-inspired approaches, such as detecting multiple spectral bands within a single pixel.

As is shown in [48] and [53], the photodiode detectivity can be estimated by the relation:

$$D^* \propto \left(\frac{\alpha}{G_{th}}\right)^{1/2} = \left(\frac{\alpha N_{maj}\tau}{n_i^2}\right)^{1/2} = \left(\frac{\sqrt{N_{maj}}}{n_i}\right)\sqrt{\alpha\tau}, \qquad (2)$$

where α – the absorption coefficient, and G_{th} (in cm^{-3}s^{-1}) – the thermal generation rate in the active detector region, N_{maj} – the majority carrier density, τ – the minority carrier lifetime, and n_i – the intrinsic carrier concentration. Equation (1) indicates that D^* is proportional to the square root of the absorption coefficient of the material and the carrier lifetime – the $\sqrt{\alpha\tau}$ product can be used as a criterion for the quality of the IR material. To improve the performance of an IR detector, the detector active volume must be reduced, thereby reducing the amount of heat generated. This requirement should be met without reducing the detector quantum efficiency, optical area, or detector field of view (FOV).

Since detectivity depends on the square root of $\alpha\tau$ ($D^* \propto \sqrt{\alpha\tau}$), the next two figures (Figs. 21 and 22) show typical room-temperature values of fundamental material parameters, such as the absorption coefficient, carrier lifetimes, and carrier mobilities.

Among narrow-gap semiconductors, the ternary alloys of mercury cadmium telluride (HgCdTe) and lead salts have the highest absorption coefficients, surpassing 10^3 cm^{-1} at the absorption threshold. InAs/GaSb type-II superlattices (T2SLs) display similar absorption characteristics, while the coefficients for InAs/InAsSb superlattices are about half of those for InAs/GaSb T2SLs [54]. In QWIPs, the relationship governing the absorption coefficient is significantly altered by low-dimensional effects, with typical values in the long-wavelength infrared (LWIR) region ranging from 600 to 800 cm^{-1}.

Generally, the impact of ionic bonding in II-VI materials is more significant compared to the strong covalent bonding in III-V materials, which enhances the confinement of electron wave functions around lattice atoms. Additionally, II-VI compounds are more adept at resisting lattice defects stemming from imperfections in crystal structure. Consequently, SRH lifetimes in low-doped HgCdTe (about 10^{13} cm^{-3}) are over three orders of magnitude longer than those observed in III-V alloys with comparable band gaps. In InAs/GaSb T2SLs, the SRH mechanism influences carrier lifetimes, typically resulting in values below 100 ns [55]. In contrast, the lack of gallium in the mid-wavelength infrared (MWIR) InAs/InAsSb superlattices contributes to significantly longer lifetimes, which can reach up to 10 µs. In LWIR QWIP devices,

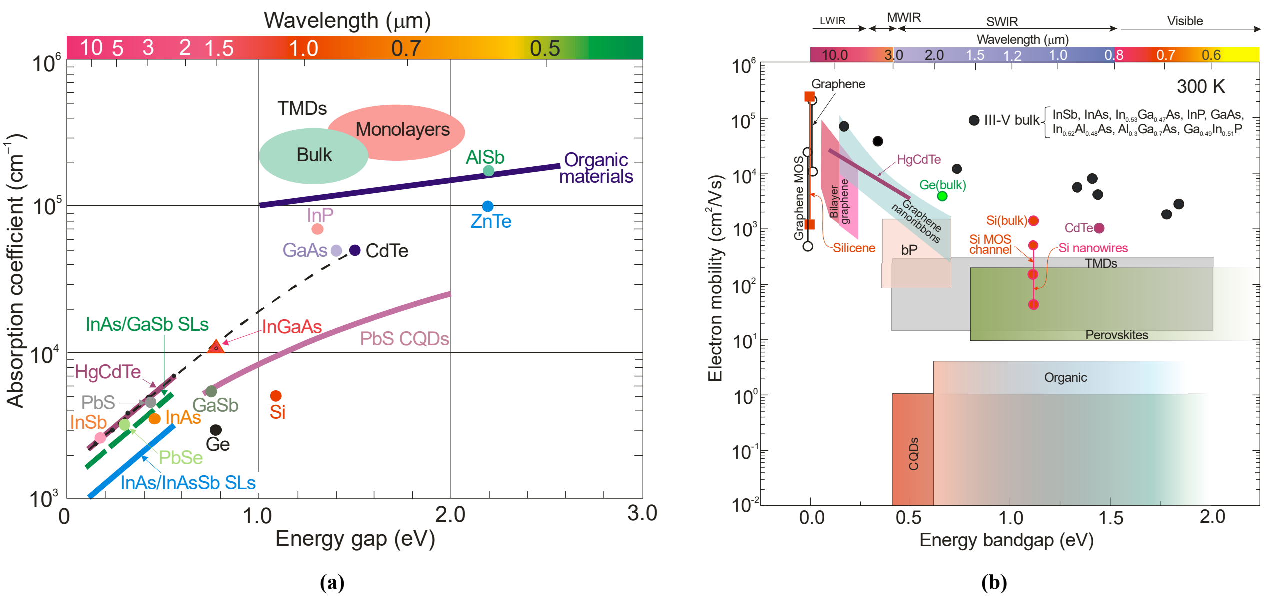

Fig. 21. Absorption coefficient (a) and electron mobilities (b) at room temperature as a function of the band gap energy for selected semiconductor materials (after [48]). The absorption coefficient was estimated for the threshold energy of $1.2 \times E_g$, where E_g is the semiconductor band gap.

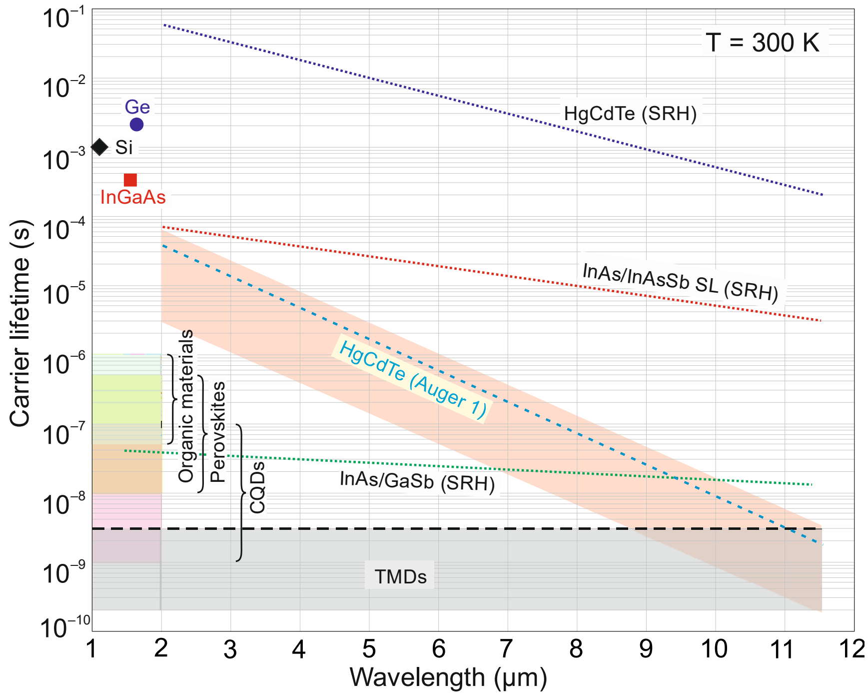

Fig. 22. Comparison of room-temperature carrier lifetimes of various layered material systems with standard semiconductors used in the manufacture of IR detectors ($A^{III}B^{V}$ compounds and ternary HgCdTe alloys) (after [48]).

longitudinal optical (LO) phonons are essential for intersubband (IS) relaxation, leading to carrier relaxation times of typically around 10 ps. Due to various physical constraints, funding for QWIP technologies has recently decreased significantly [56].

Interband-quantum cascade detectors (IB-QCDs) based on T2SL materials feature a complex detector architecture. Their design is particularly pronounced for HOT operations, with performance comparable to HgCdTe [57]. However, their challenging technology (with multiple interfaces and stressed thin films) results in high production costs.

I will assess the square root of alpha tau values for various materials based on their fundamental photoelectric properties in three IR spectral ranges: near-infrared (NIR, $\lambda_c = 1.6$ µm), mid-wavelength infrared (MWIR, $\lambda_c = 5$ µm), and long-wavelength infrared (LWIR, $\lambda_c = 10$ µm), as shown in Table 2. The reasoning behind the selected parameters for each material system is outlined in a recently published study [48]. For NIR materials (InGaAs, HgCdTe), the values of $\sqrt{\alpha\tau}$ are quite comparable. However, in the longer wavelengths of the MWIR and LWIR, HgCdTe offers a superior figure of merit relative to other material systems. Additionally, the $\sqrt{\alpha\tau}$ metric indicates that traditional materials (InGaAs, HgCdTe, and T2SL) outperform emerging next-generation photodetectors, including transition metal dichalcogenides (TMDs), perovskites, and other low-dimensional semiconductors (LDS) [48].

Figure 23 shows the spectral dependence of the photodetector detectivity at room temperature up to 20 micrometers, with a wide range of IR detectors dominating the commercial market (PV-Ge, PV-InGaAs, thermal detectors, and PV-HgCdTe) [51]. Among the new generation of devices, colloidal quantum dot (CQD)

Table 2.
Estimated $\sqrt{\alpha\tau}$ figure of merit for IR material systems at room temperature and wavelengths $\lambda = 1.6$, 5, and 10 µm.

λ [µm]	Material system	Material parameters			$\sqrt{\alpha\tau}$ [(s/cm)$^{1/2}$]
		Doping [cm^{-3}]	α [cm^{-1}]	τ	
1.6	InGaAs	5×10^{14}	1×10^{4}	200 ms	1.4
	HgCdTe	5×10^{13}	1×10^{4}	1 ms	3.2
5.0	$InAs_{0.91}Sb_{0.09}$	1×10^{15}	3.2×10^{3}	10 ms	0.18
	HgCdTe	5×10^{13}	3.2×10^{3}	1 ms	1.8
	InAs/GaSb SLs	5×10^{14}	2.4×10^{3}	20 ns	6.9×10^{-3}
	InAs/InAsSb SLs	5×10^{14}	1.2×10^{3}	2 µs	4.9×10^{-2}
	PbSe	1×10^{17}	3×10^{3}	10 ns	2.0×10^{-2}
10.0	HgCdTe	5×10^{13}	2.2×10^{3}	0.1 ms	0.47
	InAs/GaSb SLs	5×10^{14}	1.6×10^{3}	10 ns	4.0×10^{-3}
	InAs/InAsSb SLs	5×10^{14}	8.0×10^{2}	0.2 µs	1.3×10^{-2}
	GaAs/AlGaAs QWIP	5×10^{17}	7.0×10^{2}	10 ps	9.0×10^{-5}

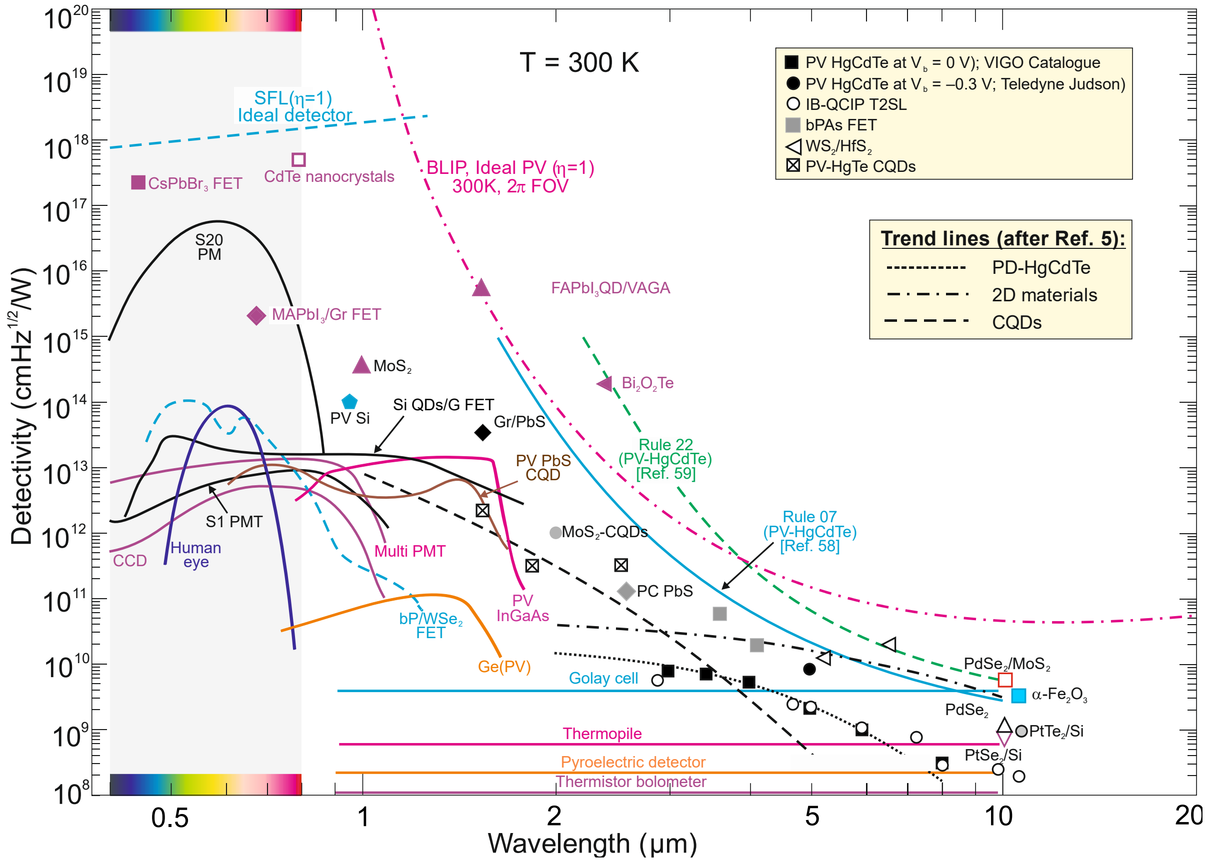

Fig. 23. Spectral dependence of detectivity for different groups of photodetectors operating at room temperature in the wavelength range of 0.5 µm to 20 µm: standard VIS (Si, CCD), and IR range detectors dominating the commercial market (PV-Ge, PV-InGaAs, thermal detectors, and PV-HgCdTe), CQD, 2D material, perovskite, and nanowire photodetectors (after [44]). The theoretical curves for the primary performance limitations of photon detectors (SFL and BLIP) are also marked. Additionally, two HgCdTe benchmarks (Rule 07 and Rule 22 [58, 59]) in the IR region are presented. PC – photoconductor, PD – photodiode, MSM – metal-semiconductor-metal, FET – field effect transistor, PM – photomultiplier, IB-QCIP – interband-quantum cascade infrared photodetector.

photodetectors, 2D material photodetectors with the best performance, and T2SL (IB-CQDPs) are also included. Additionally, Figure 23 illustrates the primary performance limitations of photon detectors, specifically the signal fluctuation limit (SFL – in wavelength range below ≈ 1.2 µm) and the background fluctuation limit, also known as the background-limited infrared photodetector (BLIP). Two curves in the IR region, marked as Rule 07 [58] and Rule 22 [59], predict photodiode HgCdTe performance and have become widely used within the IR community as reference benchmarks for alternative technologies such as III-V barrier detectors, type-II superlattice (T2SLs) devices, CQD photodetectors, and 2D material photodetectors.

The experimental results for IR photodetectors shown in Fig. 23 generally fall sub-BLIP performance standard. However, the upper performance of 2D material photodetectors is higher than that of HgCdTe photodiodes [44]. Enhancing the technology used to produce 2D materials is vital for creating advanced devices suitable for industrial applications. A significant challenge in this field is maintaining the stability and quality of these materials. Although substantial efforts have been made to improve the synthesis of large 2D monocrystals, achieving monocrystals larger than a millimeter remains difficult. While chemical vapour deposition (CVD) enables large-scale production of these samples, it often results in numerous defects and impurities, leading to degradation over time and, consequently, unstable device performance. The *in-situ* growth strategy holds promise for large-scale growth and could serve as an effective method for the future integration of 2D materials with bulk materials.

8. Conclusions

Over the course of my more than 50 years of scientific work, I have witnessed an unprecedented development in IR detectors, starting with extrinsic semiconductor detectors in the late 1960s, through the development of intrinsic narrow-gap semiconductor detectors (made of PbSnTe and HgCdTe) and alternative solid-state solutions based on III-V compounds (mainly GaAs/AlGaAs QWIPs and type-II superlattices made of InAs/GaSb and InAs/InAsSb) through next three decades. The discovery of HgCdTe in 1959 undoubtedly had the greatest impact on the development of four generations of IR detector arrays.

The main focus of ongoing research is the implementation of three technical innovations: smaller pixel pitches HOT detectors [especially in the IR spectral region] and AI. AI, in turn, is being used in conjunction with imaging in various autonomous systems for signal detection. AI-driven adaptive sensor systems could enhance real-time image processing, improve signal interpretation, and enable bio-inspired solutions, such as multi-spectral detection in a single pixel. It is expected that a new generation of photodetectors based on low-dimensional materials that have emerged over the past two decades can help develop next-generation imaging systems.

Although photodetection platforms based on LDS materials have demonstrated a variety of potential applications, outstanding challenges remain to fully exploit their distinct advantages. The prospects for commercialisation will not depend solely on the performance of a single detector, but also on the distinct advantages of being able to fabricate large-scale, high-quality materials at a low cost. The ultimate goal is to achieve a large-scale integration of LDS with existing photonic and electronic platforms, such as CMOS. It is expected that further integration of Si CMOS technology with 2D materials will increase chip functionality.

In this paper, I have sought to present my contribution to the development of IR detectors. In conclusion, I would like to mention my papers on topics that go beyond IR detectors and are well recognised in the global literature concerning ultraviolet and terahertz detectors (e.g., [60–62]).

References

[1] Norton, P. R. Infrared detectors in the next millennium. *Proc. SPIE* **3698**, Infrared Technology and Applications XXV, 652–665 (1999). https://doi.org/10.1117/12.354568

[2] Moore, G. E. Cramming more components onto integrated circuits. *Electronics* **38**, 114 (1965). https://doi.org/10.1109/N-SSC.2006.4785860

[3] Patel, C. K. N. Continuous-wave laser action on vibrational-rotational transitions of CO_2. *Phys. Rev*. **136**, A1187–A1193 (1964). https://doi.org/10.1103/PhysRev.136.A1187

[4] Małachowski, M. J. & Rogalski, A. Technologia i właściwości fotoprzewodzącego detektora promieniowania podczerwonego na GaAs. *Biuletyn WAT* (*Bull. MUT*) **XXII**, 247 (1973). (In Polish)

[5] Lawson, W. D., Nielson, S., Putley, E. H. & Young, A. S. Preparation and properties of HgTe and mixed crystals of HgTe-CdTe. *J. Phys. Chem. Solids* **9**, 325–329 (1959). https://doi.org/10.1016/0022-3697(59)90110-6

[6] Dimmock, J. O., Melngailis, I. & Strauss, A. J. Band structure and laser action in PbSnTe. *Phys. Rev. Lett*. **16**, 1193–1196 (1966). https://doi.org/10.1103/PhysRevLett.16.1193

[7] Rogalski, A. & Ziencik, H. Technologia – struktura i własności warstw $Pb_{0.82}Sn_{0.18}Te$ otrzymywanych zmodyfikowaną techniką gorącego kanału. *Biuletyn WAT* (*Bull. MUT*) **XXVI**, 302 (1977). (in Polish)

[8] Zięcik, H. & Rogalski, A. The preparation, structure and properties of $Pb_{0.82}Sn_{0.18}Te$ films obtained by modified hot-wall evaporation technique. *Electron Technol.* **11**, 69–74 (1978).

[9] Lopez-Otero, A. HOT wall epitaxy. *Thin Solid Films* **49**, 3–57 (1978). https://doi.org/10.1016/0040-6090(78)90309-7

[10] Rogalski, A. n-PbTe/p^+-$Pb_{1-x}Sn_xTe$ heterojunctions prepared by a modified hot wall technique. *Thin Solid Films* **67**, 179–186 (1980). https://doi.org/10.1016/0040-6090(80)90302-8

[11] Rogalski, A., Piotrowski, J., & Gronkowski, J. A modified hot wall epitaxy technique for the growth of CdTe and $Hg_{1-x}Cd_xTe$ epitaxial layer. *Thin Solid Films* **191**, 239–245 (1990). https://doi.org/10.1016/0040-6090(90)90376-O

[12] Rogalski, A. Właściwości optyczne warstw $Pb_{1-x}Sn_xTe$ w temperaturze pokojowej. *Biuletyn WAT* (*Bull. MUT*) **XXV**, 284 (1976). (in Polish)

[13] Jäger, H. & Schubert, G. Infrared refractive indices of $Pb_{1-x}Sn_xTe$ alloys at room temperature. *Infrared Phys.* **13**, 29–36 (1972). https://doi.org/10.1016/0020-0891(73)90006-7

[14] Igras, E. & A. Rogalski, A. Electrical and photoelectrical properties of (n)PbTe-(p)$Pb_{0.82}Sn_{0.18}Te$ heterojunctions. *Electron Technol.* **30**(4), 71–79 (1977).

[15] Rogalski, A. Detektory fotowoltaiczne $Pb_{1-x}Sn_xTe$ okna atmosferycznego 8–14 µm otrzymywane zmodyfikowaną techniką gorącego kanału. *Biuletyn WAT* (*Bull. MUT*) **XXVIII**, 324 (1979). (in Polish)

[16] Fujiyasu, H. *et al*. Optical and electrical properties of PbTe-$Pb_{1-x}Sn_xTe$ superlattices prepared on KC1 by a HWE. *Surf. Sci.* **142** 579–585 (1984). https://doi.org/10.1016/0039-6028(84)90364-9

[17] Bauer G. & Kriechbaum, M. Properties of PbTe/$Pb_{1-x}Sn_xTe$ superlattices. in *Optical Properties of Narrow-Gap Low-Dimensional Structures* (eds. Sotomayor Torres, C. M., Portal, J. C., Maan, J. C. & Stradling, R. A.) vol. 157 (NATO ASI Series, Springer, 1987). https://doi.org/10.1007/978-1-4613-1879-8_10

[18] Baars, J. New aspects of the material and device technology of intrinsic infrared photodetectors. in *Physics of Narrow Gap Semiconductors* (eds. Gornik, E., Heinrich, H. & Palmetshofer, L.) 280–282 (Springer, Berlin, 1982). https://doi.org/10.1007/3-540-11191-3_47

[19] Rogalski A. & Larkowski, W. Comparison of photodiodes for the 3–5.5 µm and 8–12 µm spectral regions. *Electron Technol.* **18**, 55–69 (1985).

[20] Bubulac, L. O. *et al*. P-on-n arsenic-activated junctions in MOCVD LWIR HgCdTe/GaAs. *Semiconductor. Sci. Technol*. **5**, S45–S48 (1990). https://doi.org/10.1088/0268-1242/5/3S/011

[21] Rogalski, A. History of HgTe-based photodetectors in Poland. *Opto-Electron. Rev.* **18**, 284–294 (2010). https://doi.org/10.2478/s11772-010-1025-8

[22] Piotrowski, J. *et al*. Composition and thickness control of $Cd_xHg_{1-x}Te$ layers grown by open tube isothermal vapour phase epitaxy. *J. Cryst. Growth* **83**, 122–126 (1987). https://doi.org/10.1016/0022-0248(87)90512-4

[23] Gawron, W. *et al*. The performance of the ICIP Ga-free superlattice longwave infrared photodetector for high operating temperature. *Infrared Phys. Technol*. **128**, 104499 (2023). https://doi.org/10.1016/j.infrared.2022.104499

[24] Gawron, W. *et al*. Demonstration of T2SLs InAs/InAsSb based interband cascade detector supported by immersion lens for LWIR. *J. Electron. Mater*. **52**,7068–7073 (2023). https://doi.org/10.1007/s11664-023-10665-7

[25] Rogalski, A. $Hg_{1-x}Zn_xTe$ as a potential infrared detector material. *Prog. Quantum Electron.* **13**, 299–353 (1989). https://doi.org/10.1016/0079-6727(89)90008-6

[26] Rogalski, A. $Hg_{1-x}Mn_xTe$ as a new infrared detector material. *Infrared Phys.* **31**, 117–166 (1991). https://doi.org/10.1016/0020-0891(91)90064-M

[27] Rogalski, A. *New Ternary Alloy Systems for Infrared Detectors.* (SPIE Press, Bellingham, WA, 1994).

[28] Sher, A., Chen, A.-B., Spicer, W. E. & Shih, C.-K. Effects influencing the structural integrity of semiconductors and their alloys. *J. Vac. Sci. Technol.* **A3**, 105–111 (1985). https://doi.org/10.1116/1.573177

[29] Woolley, J. C. & Smith, B. A. Solid solution in III-V compounds. *Proc. Phys. Soc.* **72**, 214–223 (1958). https://doi.org/10.1088/0370-1328/72/2/306

[30] Cheung, D. T. *et al.* Backside-illuminated $InAs_{1-x}Sb_x$-InAs narrow-band photodetectors. *Appl. Phys. Lett.* **30**, 587–598 (1977). https://doi.org/10.1063/1.89246

[31] Rogalski, A. InAsSb infrared detectors. *Prog. Quantum Electron.* **13**, 191–231 (1989). https://doi.org/10.1016/0079-6727(89)90003-7

[32] Rogalski, A., Kopytko, M. & Martyniuk, P. *Antimonide-Based Infrared Detectors. A New Perspective.* (SPIE Press, Bellingham, 2018). https://doi.org/10.1117/3.2278814

[33] Rogalski, A. & Piotrowski, J. Intrinsic infrared detectors. *Prog. Quantum Electron.* **12**, 87–289 (1988). https://doi.org/10.1016/0079-6727(88)90001-8

[34] Rogalski, A. Homepage. https://antonirogalski.com/

[35] Esaki, L. & Tsu, R. Superlattice and negative conductivity in semiconductors. *IBM J. Res. Dev.* **14**, 61–65 (1970). https://doi.org/10.1147/rd.141.0061

[36] A. Rogalski. Quantum well photoconductors in infrared detectors technology. *J. Appl. Phys.* **93**, 4355–4391 (2003). https://doi.org/10.1063/1.1558224

[37] Rogalski, A. Comparison of the performance of quantum well and conventional bulk infrared photodetectors. *Infrared Phys. Technol.* **38**, 295–310 (1997). https://doi.org/10.1016/S1350-4495(97)00015-7

[38] Andersson, J. Y. Dark current mechanisms and conditions of background radiation limitation of n-doped AlGaAs/GaAs quantum-well infrared detectors. *J. Appl. Phys.* **78**, 6298–6304 (1995). https://doi.org/10.1063/1.360510

[39] Singh, A. & Manasreh, M. O. Quantum well and superlattice heterostructures for space-based long wavelength infrared photodetectors. *Proc. SPIE* **2397**, 193–209 (1995). https://doi.org/10.1117/12.206869

[40] Rogalski, A. & Martyniuk, P. InAs/GaInSb superlattices as a promising material system for third generation infrared detectors. *Infrared Phys. Technol.* **48**, 39–52 (2006). https://doi.org/10.1016/j.infrared.2005.01.003

[41] Rogalski, A. Graphene-based materials in the infrared and terahertz detector families: A tutorial. *Adv. Opt. Photonics* **11**, 314–379 (2019). https://doi.org/10.1364/AOP.11.000314

[42] Rogalski, A. *2D Materials for Infrared and Terahertz Detectors.* (CRC Press, Boca Raton, 2021). https://doi.org/10.1201/9781003043751

[43] Rogalski, A. Van der Waals materials for HOT infrared detectors: A review. *Opto-Electro. Rev.* **30**, e140558 (2022). https://doi.org/10.24425/opelre.2022.140551

[44] Rogalski, A., Kopytko, M., Hu, W. & Martyniuk, P. Infrared HOT photodetectors: Status and outlook. *Sensors* **23**, 7564 (2023). https://doi.org/10.3390/s23177564

[45] Rogalski, A. A look at the future of perovskite detectors. *Appl. Phys. Lett.* **125**, 090501 (2024). https://doi.org/10.1063/5.0228001

[46] Rogalski, A., Hu, W., Wang, F., Wang, Y. & Martyniuk, P. Perovskite versus standard photodetectors. *Materials* **17**, 4029 (2024). https://doi.org/10.3390/ma17164029

[47] Rogalski, A., Hu, W., Wang, F. & Martyniuk, P. Performance of low-dimensional solid room-temperature photodetectors – Critical view. *Materials* **17**, 4522 (2024). https://doi.org/10.3390/ma17184522

[48] Rogalski, A. α/G figure of merit for infrared photodetector materials. *J. Appl. Phys*. **137**, 170701 (2025). https://doi.org/10.1063/5.0260949

[49] Rogalski, A. *et al*. Peculiarities of room temperature organic photodetectors. *Light Sci. Appl.* **14**, 359 (2025). https://doi.org/10.1038/s41377-025-01939-2

[50] Rogalski, A., Hu, W. & Martyniuk, P. *Room Temperature Photon Detectors.* (CRC Press, Boca Raton, 2025). https://doi.org/10.1201/9781003469919

[51] Rogalski, A. Evolution in the development of photodetectors: From ultraviolet to terahertz. *Appl. Phys. Rev.* **13**, 011316 (2026). https://doi.org/10.1063/5.0288436

[52] Karwowski, M. Prezes Rady Ministrów nagrodził naukowców. Forum Akademickie. https://forumakademickie.pl/prezes-rady-ministrow-nagrodzil-naukowcow/ (2024) (in Polish)

[53] Piotrowski, J. & Rogalski, A. Comment on “Temperature limits on infrared detectivities of $InAs/In_xGa_{1-x}Sb$ superlattices and bulk $Hg_{1-x}Cd_xTe$” [J. Appl. Phys. **74**, 4774 (1993)]. *J. Appl. Phys*. **80**, 2542–2544 (1996). https://doi.org/10.1063/1.363043

[54] Klipstein, P. C. *et al*. Modeling InAs/GaSb and InAs/InAsSb superlattice infrared detectors. *J. Electron. Mater*. **43**, 2984–2990 (2014). https://doi.org/10.1007/s11664-014-3169-3

[55] Rogalski, A., Martyniuk, P. and Kopytko, M. Type-II superlattice photodetectors versus HgCdTe photodiodes. *Prog. Quantum Electron*. **68**, 100228 (2019). https://doi.org/10.1016/j.pquantelec.2019.100228

[56] Jhabvala, M., Choi, K.-K., Gunapala, S., Razeghi, M. & Sundaram, M. QWIPs, SLS, Landsat and the international space station. *Proc. SPIE* **11288**, 1128802 (2020). https://doi.org/10.1117/12.2539147

[57] Martyniuk, P., Rogalski, A. & Krishna, S. Interband quantum cascade infrared photodetectors: Current status and future trends. *Phys. Rev. Appl.* **17**, 027001 (2022). https://doi.org/10.1103/PhysRevApplied.17.027001

[58] Tennant, W. E., Lee, D., Zandian, M., Piquette, E. & Carmody, M. MBE HgCdTe technology: A very general solution to IR detection, described by ‘Rule 07’, a very convenient heuristic. *J. Electron. Materials* **37**, 1406–1410 (2008). https://doi.org/10.1007/s11664-008-0426-3

[59] Zandian, M. Rule-22: An update to Rule-07. *J. Electron. Mater*. **52**, 7095–7102 (2023). https://doi.org/10.1007/s11664-023-10715-0

[60] Razeghi, M. & Rogalski, A. Semiconductor ultraviolet detectors. *J. Appl. Phys*. **79**, 7433–7473 (1996). https://doi.org/10.1063/1.362677

[61] Rogalski, A. & Sizov, F. Terahertz detectors and focal plane arrays. *Opto-Electron. Rev*. **19**, 346–404 (2011). https://doi.org/10.2478/s11772-011-0033-3

[62] Rogalski, A. *Infrared and Terahertz Detectors.* (CRC Press, Boca Raton, 2020). https://doi.org/10.1109/MIE.2019.2929349